

PASSIVE MILLIMETER-WAVE IMAGING WITH EXTENDED DEPTH OF FIELD AND SPARSE DATA

Vishal M. Patel¹ and Joseph N. Mait²

¹Center for Automation Research, UMIACS
University of Maryland, College Park, MD

²U.S. Army Research Laboratory, Adelphi, MD
pvishalm@umiacs.umd.edu joseph.mait@us.army.mil

ABSTRACT

In this paper, we introduce a new millimeter wave imaging modality with extended depth-of-field that provides diffraction limited images based on a significant reduction in scan-time. The technique uses a cubic phase element in the pupil of the system and a non-linear recovery algorithm to produce images that are insensitive to object distance. We present experimental results that validate system performance and demonstrate a greater than four-fold increase in depth-of-field with a reduction in scan-time by a factor of at least two.

Index Terms— Computational imaging, millimeter wave imaging, extended depth-of-field, image reconstruction, sparsity.

1. INTRODUCTION

Over the past several years, imaging using millimeter wave (mmW) and terahertz technology has gained a lot of interest [1], [2], [3]. This interest is, in part, driven by the ability to penetrate poor weather and other obscuring materials such as clothes and polymers. Millimeter waves are high-frequency electromagnetic waves usually defined to be in the 30 to 300 GHz range with corresponding wavelengths between 10 to 1mm. Radiation at these frequencies is non-ionizing and is safe to use on people. Applications of this technology include the detection of concealed weapons, explosives and contraband. Fig. 1 compares a visible image and corresponding 94-GHz image of two people with various weapons concealed under clothing. Note that concealed weapons are clearly detected in the mmW image.

Recently, in [3], Mait *et al.* presented a computational imaging method to extend the depth-of-field of a passive mmW imaging system. The method uses a cubic phase element in the pupil plane of the system to render system operation relatively insensitive to object distance. The aberrations introduced by the cubic phase elements are then removed by post-detection signal processing. It was shown that, one can increase the depth-of-field of a 94GHz imager four times its normal depth-of-field [3].

Several other systems have also been developed and discussed in the literature [1], [2]. Some of them use a single-beam system that forms an image by scanning in azimuth and elevation. One of the main drawbacks of mechanical scanning is that it significantly limits the acquisition speed. For instance, it takes about 15 seconds for a 94-GHz imager to scan a 30°-by-30° angular sector. Real-time mmW imaging has also been demonstrated using an array of sensors. However, these systems introduce higher complexity and

are costly. To deal with this, compressive sampling methods [4], [5] have been applied to mmW imaging which reduces the number of samples required to form an image [6], [7], [8], [9], [10], [11].



Fig. 1. Millimeter wave imaging through clothing. (a) Visible image of the scene. (b) Image produced using a 94-GHz imaging system.

In this paper, we describe a passive mmW imaging system with extended depth-of-field that can produce images with reduced number of samples. We show that if the mmW image is assumed to be sparse in some transform domain, then one can reconstruct a good estimate of the image using this new image formation algorithm. Our method relies on using a far fewer number of measurements than the conventional systems do and can reduce the scan-time significantly.

The organization of the paper is as follows. Section 2 provides background information on passive mmW imaging using a 94GHz system. The proposed undersampling scheme is described in Section 3. We demonstrate experimental results in Section 4 and Section 5 concludes the paper with a brief summary and discussion.

2. BACKGROUND

A schematic diagram of our mmW imaging system is shown in Fig. 2. It is a 94-GHz Stokes-vector radiometer used for mmW measurements. It is a single-beam system that produces images by scanning in horizontal and vertical axis. The radiometer has a thermal sensitivity of 0.3 K with a 30-ms integration time and 1-GHz bandwidth per pixel. A Cassegrain antenna is mounted to the front of the radiometer receiver that has 24" diameter primary parabolic reflector and a 1.75" diameter secondary hyperbolic reflector. The position of the hyperbolic secondary is variable.

One can model the 94-GHz imaging system as a linear, spatially incoherent, quasi-monochromatic system [3]. The intensity of the detected image can be represented as a convolution between the intensity of the image predicted by the geometrical optics with the

This work was partially supported by a MURI from the Army Research Office under the Grant W911NF-09-1-0383.

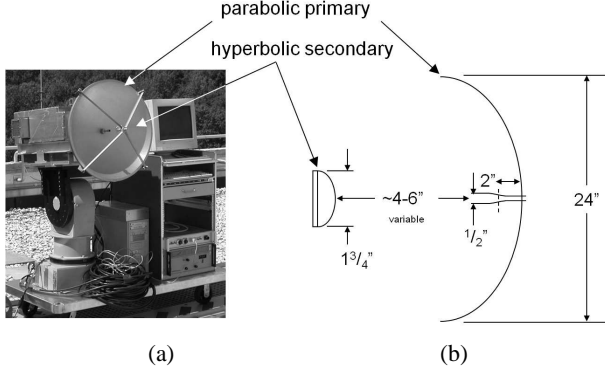


Fig. 2. 94-GHz imaging system. (a) Image of the scanning system. (b) Schematic diagram with measured dimensions.

system point spread function [12]

$$ii(x, y) \triangleq |i(x, y)|^2 = o_g(x, y) ** h(x, y), \quad (1)$$

where $**$ represents the two-dimensional convolution operation. The function $o_g(x, y)$ represents the inverted, magnified image of the object that a ray-optics analysis of the system predicts.

The second term in (1), $h(x, y)$, is the incoherent point spread function (PSF) that accounts for wave propagation through the aperture

$$h(x, y) = \frac{1}{(\lambda f)^4} \left| p\left(\frac{-x}{\lambda f}, \frac{-y}{\lambda f}\right) \right|^2, \quad (2)$$

where $p(x/\lambda f, y/\lambda f)$ is the coherent point spread function. The function $p(x, y)$ is the inverse Fourier transform of the system pupil function $P(u, v)$

$$p(x, y) = FT^{-1}[P(u, v)].$$

Without loss of generality, assume the recorded arrays are of size $N \times N$. Then, eq. (1) can be described as

$$\mathbf{i} = \mathbf{H}\mathbf{o}_g, \quad (3)$$

where \mathbf{i} and \mathbf{o}_g are $N^2 \times 1$ lexicographically ordered column vectors representing the $N \times N$ arrays $ii(x, y)$ and $o_g(x, y)$, respectively, and \mathbf{H} is the $N^2 \times N^2$ matrix that models the incoherent point spread function $h(x, y)$. Displacement, d_ϵ , of an object from the nominal object plane introduces a phase error, $\theta_\epsilon(u, v)$, in the pupil function. The phase error increases the width of a point response.

The system's depth-of-field (DoF) is defined as the distance in object space over which an object can be placed and still produce an in-focus image. For a 94 GHz imager with an aperture diameter $D = 24''$ and object distance $d_o = 180''$, $DoF \approx 17.4''$ which ranges from $175.2''$ to $192.6''$ [3].

The cubic phase element $P_c(u, v)$ is

$$P_c(u, v) = \exp(j\theta_c(u, v)) \text{rect}\left(\frac{u}{W_u}, \frac{v}{W_v}\right), \quad (4)$$

where

$$\theta_c(u, v) = (\pi\gamma) \left[\left(\frac{2u}{W_u}\right)^3 + \left(\frac{2v}{W_v}\right)^3 \right]$$

and rect is the rectangular function. The phase function is separable in the u and v spatial frequencies and has spatial extent W_u and

W_v along the respective axis. The constant γ represents the strength of the cubic phase. Fig. 3 shows the measured PSFs for conventional imaging and imaging with a cubic phase. Note that the response of the cubic phase system is relatively unchanged, whereas the response of the conventional system changes considerably.

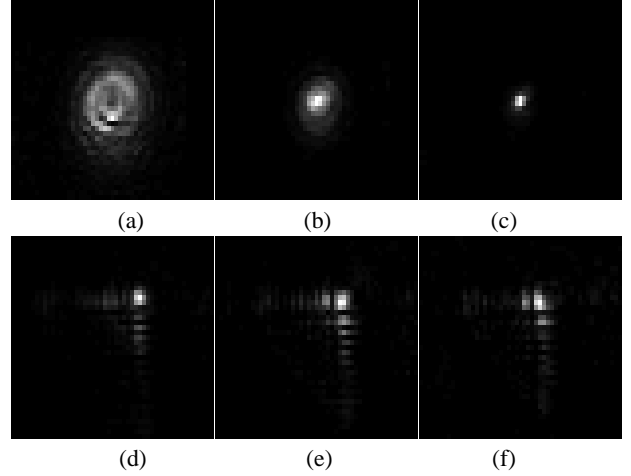


Fig. 3. Measured point spread functions for conventional imaging and imaging with a cubic phase. PSFs for conventional system at (a) 113'', (b) 146.5'', and (c) 180''. (d)-(f) PSFs for a system with cubic phase at the same distances for (a)-(c).

A post-detection signal processing step is usually employed to remove the artifacts of the aberrations introduced by the cubic phase element to produce a well-defined sharp response [13], [14], [15]. Assuming a linear process

$$i_p(x, y) = ii(x, y) ** w(x, y) \quad (5)$$

one can implement $w(x, y)$ as a Wiener filter in the Fourier space

$$W(u, v) = \frac{H_c^*(u, v)}{|H_c(u, v)|^2 + \frac{K^{-2}\hat{\Phi}_N(u, v)}{\hat{\Phi}_L(u, v)}}, \quad (6)$$

where $H_c(u, v)$ is the optical transfer function associated with the cubic phase element, the parameter K is a measure of the signal-to-noise ratio, the functions $\hat{\Phi}_L$ and $\hat{\Phi}_N$ are the expected power spectra of the object and noise, respectively. The optical transfer function is usually estimated from the experimentally measured point responses. One can view the estimated i_p as a diffraction limited response. In the matrix notation, one can rewrite eq.(5) as

$$\mathbf{i}_p = \mathbf{W}\mathbf{i} = \mathbf{W}\mathbf{H}\mathbf{o}_g, \quad (7)$$

where \mathbf{i}_p is the $N^2 \times 1$ column vector corresponding to array $i_p(x, y)$ and \mathbf{W} is the $N^2 \times N^2$ convolution matrix corresponding to the Wiener filter $w(x, y)$.

3. ACCELERATED IMAGING WITH EXTENDED DEPTH-OF-FIELD

Since our objective is to form mmW images with reduced number of samples, we propose the following sampling strategy. Our sensor is a single-beam system that produces images by scanning in azimuth and elevation. One can reduce the number of samples by randomly

undersampling in both azimuth and elevation. Mathematically, this amounts to introducing a mask in eq. (1) as follows

$$\mathbf{i}_M = \mathbf{M}\mathbf{i} = \mathbf{M}\mathbf{H}\mathbf{o}_g, \quad (8)$$

where \mathbf{i}_M is an $N^2 \times 1$ lexicographically ordered column vector of observations with missing information. Here, \mathbf{M} is the degradation operator that removes the p samples from the signal. This matrix is of size $N^2 \times N^2$, built by taking the $N^2 \times N^2$ identity matrix with p zeros in the diagonal correspond to the discarded samples.

To remove the artifacts of the aberrations introduced by the cubic phase element a Wiener filter can be implemented as shown in eq. (5). Then, the observation model can be written as

$$\mathbf{i}_o = \mathbf{W}\mathbf{i}_M = \mathbf{W}\mathbf{M}\mathbf{i} = \mathbf{W}\mathbf{M}\mathbf{H}\mathbf{o}_g. \quad (9)$$

Using the relation in eq. (7), one can write $\mathbf{H}\mathbf{o}_g$ in terms of the diffraction limited response, \mathbf{i}_p , as

$$\mathbf{H}\mathbf{o}_g = \mathbf{G}\mathbf{i}_p, \quad (10)$$

where, \mathbf{G} is the regularized inverse filter corresponding to \mathbf{W} . With this, and assuming the presence of additive noise η , one can rewrite the observation model (9) as

$$\mathbf{i}_o = \mathbf{W}\mathbf{M}\mathbf{G}\mathbf{i}_p + \eta, \quad (11)$$

where η denotes the $N^2 \times 1$ column vector corresponding to noise, η . We assume that $\|\eta\|^2 = \epsilon^2$.

Having observed \mathbf{i}_o and knowing the matrices \mathbf{W} , \mathbf{M} and \mathbf{G} , the general problem is to estimate the diffraction limited response, \mathbf{i}_p . Assume that \mathbf{i}_p is sparse or compressible in a basis or frame Ψ so that $\mathbf{i}_p = \Psi\alpha$ with $\|\alpha\|_0 = K \ll N^2$, where the ℓ_0 sparsity measure $\|\cdot\|_0$ counts the number of nonzero elements in the representation. The observation model (11) can now be rewritten as

$$\mathbf{i}_o = \mathbf{W}\mathbf{M}\mathbf{G}\Psi\alpha + \eta. \quad (12)$$

This is a classic inverse problem whose solution can be obtained by solving the following optimization problem

$$\hat{\alpha} = \arg \min_{\alpha} \|\alpha\|_1 \quad \text{subject to} \quad \|\mathbf{i}_o - \mathbf{W}\mathbf{M}\mathbf{G}\Psi\alpha\|_2 \leq \epsilon. \quad (13)$$

Once the representation vector α is estimated, we obtain the final estimate of \mathbf{i}_p as $\hat{\mathbf{i}}_p = \Psi\hat{\alpha}$. Note that the recovery of α from eq. (12) will depend on certain conditions on the sensing matrix $\mathbf{W}\mathbf{M}\mathbf{G}\Psi$ and the sparsity of α [16].

4. EXPERIMENTAL RESULTS

In this section, we demonstrate the performance and applicability of our method on simulated data with the measured PSFs. In these experiments, we use an orthogonal wavelet transform (Daubechies 4 wavelet) as a sparsifying transform. There has been a number of approaches suggested for solving optimization problems such as eq. (13). In our approach, we employ a highly efficient algorithm that is suitable for large scale applications known as the Gradient Projection for Sparse Reconstruction (GPSR) algorithm [17].

The extended object used in our experiments is represented in Fig. 4(a). Images of an extended object for conventional imaging system at 113", 146" and 180" are shown in Fig. 5(a)-(c), respectively. Note that the conventional imaging system produces images with significant blurring. In contrast, even without signal processing, the images produced with cubic phase element retain more discernable characteristics of the object than the images from the conventional system, as shown in Fig. 5(d)-(f). It can be seen from

Fig. 5(g)-(i) that post processing removes the artifacts of aberrations introduced by the cubic phase element and produces sharp images. Hence, one can extend the region over which the system generates diffraction limited images. In fact, in [3], it was shown that the DoF of a conventional 94GHz imaging system can be extended from 17.4" to more than 68".

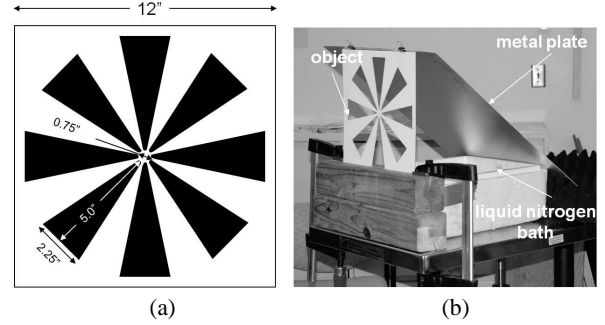


Fig. 4. (a): Representation of the extended object used to compare conventional and cubic-phase imaging. (b): Schematic of object illumination.

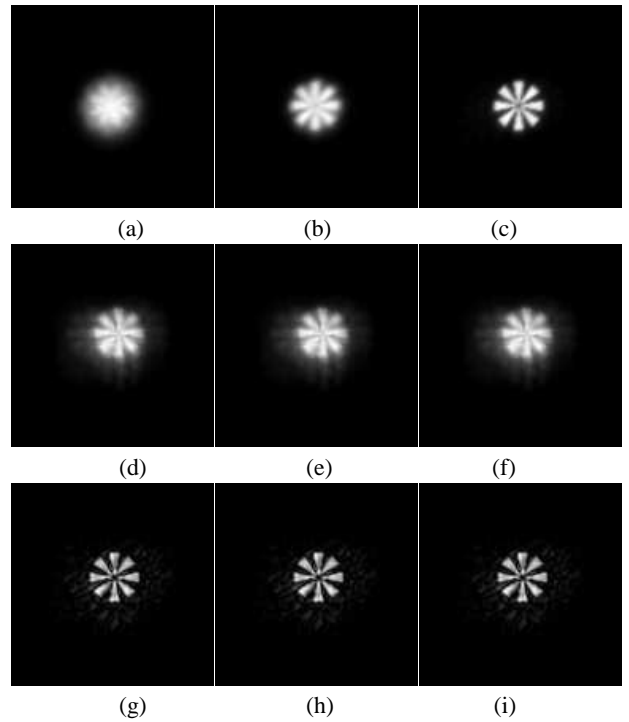


Fig. 5. Images from a conventional imaging system at (a) 113", (b) 146" and (c) 180". (d)-(f) Images from a system with cubic phase at the same object distances as for (a)-(c). (g)-(i) Processed images from a system with cubic phase at the same object distances as for (a)-(c).

Fig. 7(a)-(c) show the sparsely sampled cubic phase data. Only 50% of the data is sensed. The samples were discarded according to a random undersampling pattern shown in Fig. 6(a). This corresponds to a reduction in scan-time by a factor of 2. The reconstructed images obtained by solving problem (13) are shown in Fig. 7(d)-(f).

The reconstructions of the extended object are comparable to the processed images from a system with cubic phase. This can be seen by comparing Fig. 5(g)-(i) with Fig. 7(d)-(f).

In Fig. 6(b), shows the peak-signal-to-noise-ratio (PSNR) curves as we vary the number of measurements. We see that with increase in number of measurements the reconstruction quality generally improves. It is interesting to note that the PSNR values stay about the same after 50% of the measurements are taken. Furthermore, reconstruction curves corresponding to all three distances 113", 146" and 180" follow the similar curves, showing the depth invariance of the system. These figure shows that it is indeed possible to extended depth-of-field even when cubic phase data is sparsely sampled.

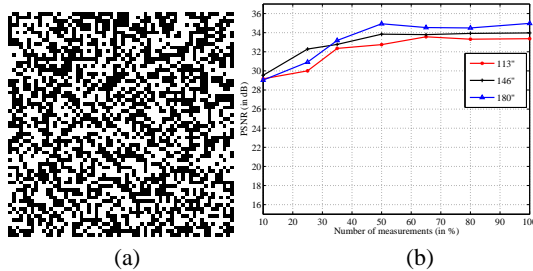


Fig. 6. (a) A random undersampling pattern. (b) Relative error vs. number of measurement curves.

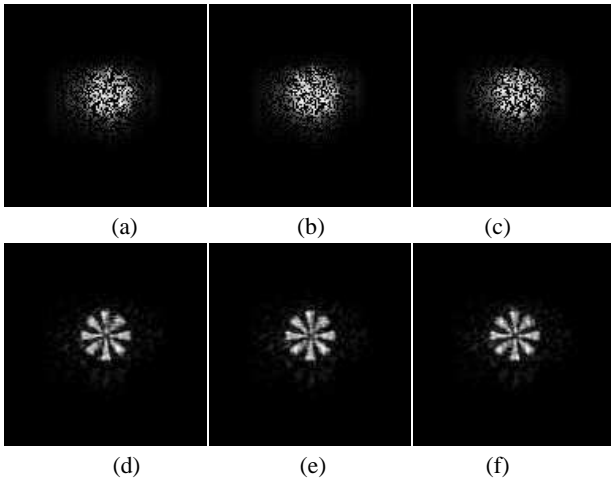


Fig. 7. Sparsely sampled data from a modified imaging system at (a) 113", (b) 146", and (c) 180". (d)-(f) Diffraction limited images recovered by solving (13) at the same object distances as for (a)-(c).

5. DISCUSSION AND CONCLUSION

We have utilized a computational imaging technique along with a nonlinear reconstruction method and demonstrated that extended depth-of-field is possible for passive millimeter wave imaging even when the cubic phase data is sparsely sampled.

Millimeter wave systems image temperature contrasts. Hence, careful analysis of noise and contrast in such systems is necessary to assess the impact of inserting a cubic phase element in the pupil plane of the system and sparsely sampling the data. More analysis on

the artifacts introduced by the cubic phase element and random undersampling in terms of the point spread function will be discussed elsewhere (see [18] for more details).

6. REFERENCES

- [1] R. Appleby and R. N. Anderton, "Millimeter-wave and submillimeter-wave imaging for security and surveillance," *Proceedings of the IEEE*, vol. 95, no. 8, pp. 1683–1690, Aug. 2007.
- [2] L. Yujiri, M. Shoucri, and P. Moffa, "Passive millimeter wave imaging," *IEEE Microwave Magazine*, vol. 4, no. 3, pp. 39–50, sept. 2003.
- [3] J. Mait, D. Wikner, M. Mirotznik, J. van der Gracht, G. Behrmann, B. Good, and S. Mathews, "94-GHz imager with extended depth of field," *IEEE Transactions on Antennas and Propagation*, vol. 57, no. 6, pp. 1713–1719, june 2009.
- [4] D. Donoho, "Compressed sensing," *IEEE Transactions on Information Theory*, vol. 52, no. 4, pp. 1289–1306, Apr. 2006.
- [5] E. Candes, J. Romberg, and T. Tao, "Robust uncertainty principles: exact signal reconstruction from highly incomplete frequency information," *IEEE Transactions on Information Theory*, vol. 52, no. 2, pp. 489–509, Feb. 2006.
- [6] S. D. Babacan, M. Luessi, L. Spinoulas, and A. K. Katsaggelos, "Compressive passive millimeter-wave imaging," in *IEEE ICIP*, 2011.
- [7] N. Gopalsami, T. W. Elmer, S. Liao, R. Ahern, A. Heifetz, A. C. Raptis, M. Luessi, S. D. Babacan, and A. K. Katsaggelos, "Compressive sampling in passive millimeter-wave imaging," in *Proc. SPIE*, vol. 8022, 2011.
- [8] C. F. Cull, D. A. Wikner, J. N. Mait, M. Mattheiss, and D. J. Brady, "Millimeter-wave compressive holography," *Appl. Opt.*, vol. 49, no. 19, pp. E67–E82, Jul 2010.
- [9] C. A. Fernandez, D. Brady, J. N. Mait, and D. A. Wikner, "Sparse fourier sampling in millimeter-wave compressive holography," in *Digital Holography and Three-Dimensional Imaging*, 2010, p. JMA14.
- [10] W. L. Chan, K. Charan, D. Takhar, K. F. Kelly, R. G. Baraniuk, and D. M. Mittleman, "A single-pixel terahertz imaging system based on compressed sensing," *Appl. Phys. Lett.*, vol. 93, no. 12, pp. 121105–3, 2008.
- [11] I. Noor, O. Furxhi, and E. L. Jacobs, "Compressive sensing for a sub-millimeter wave single pixel imager," in *Proc. SPIE*, vol. 8022, 2011.
- [12] J. W. Goodman, *Introduction to Fourier optics*. Englewood, CO: Roberts and Company, 2005.
- [13] W. T. Cathey and E. R. Dowski, "New paradigm for imaging systems," *Appl. Opt.*, vol. 41, no. 29, pp. 6080–6092, Oct. 2002.
- [14] J. Edward R. Dowski and W. T. Cathey, "Extended depth of field through wave-front coding," *Appl. Opt.*, vol. 34, no. 11, pp. 1859–1866, Apr. 1995.
- [15] S. Bradburn, W. T. Cathey, and E. R. Dowski, "Realizations of focus invariance in optical-digital systems with wave-front coding," *Appl. Opt.*, vol. 36, no. 35, pp. 9157–9166, Dec. 1997.
- [16] M. Elad, *Sparse and Redundant Representations: From theory to applications in Signal and Image processing*. Springer, 2010.
- [17] M. Figueiredo, R. Nowak, and S. Wright, "Gradient projection for sparse reconstruction: Application to compressed sensing and other inverse problems," *IEEE Journal of Selected Topics in Signal Processing*, vol. 1, no. 4, pp. 586–597, dec. 2007.
- [18] V. M. Patel, G. R. Easley, D. M. Healy, and R. Chellappa, "Compressed synthetic aperture radar," *IEEE Journal of Selected Topics in Signal Processing*, vol. 4, no. 2, pp. 244–254, april 2010.